Frequency Dependent Electrical Properties of Dunite as Functions of Temperature and Oxygen Fugacity

J.J. Roberts* and J.A. Tyburczy

Department of Geology, Arizona State University, Tempe, AZ 85287-1404, USA

Abstract. Using impedance spectroscopy, we have measured the electrical properties of two dunites and a single crystal olivine sample from 1000 to 1200° C as a function of oxygen fugacity (f_{O_2}). Two conduction mechanisms with resistances that add in series are observed for the dunites corresponding to grain interior and grain boundary conduction mechanisms. The conductivities for each mechanism were determined by analyzing the data using a complex nonlinear least squares fitting routine and the equivalent circuit approach. The grain interiors display a conductivity dependent on f_{O_2} to the $1/5.5$–$1/7$ power, consistent with other determinations, and interpreted as indicating small polaron transport ($Fe^{\cdot}_{Mg}$). The grain boundaries demonstrate a weaker f_{O_2} dependence that is dependent on temperature and material. Under certain conditions the f_{O_2} dependence of the grain boundary conductivity is negative. This result indicates that oxygen ion transport is probably not the dominant grain boundary charge transport mechanism; however, an unequivocal determination of the grain boundary mechanism has not been achieved. In some dunites the grain boundaries are more conductive than the grain interiors; in other dunites they are more resistive than grain interiors. The grain boundaries do not enhance the total conductivity of any of the materials of this study but are the controlling mechanism in some instances. Measurement of the complex electrical response at frequencies as low as 10^{-4} Hz is required to determine the role of grain boundaries on the overall electrical properties of polycrystalline dunite.

Introduction

Because of its volumetric abundance olivine is an important mineral in the upper mantle and lower crust. Our understanding of the composition, state, and dynamics of these regions depends on our understanding the physical properties of representative single and polycrystalline samples. The measurement of the electrical conductivity of single and polycrystalline olivine has led to an increased understanding of point defect chemistry and defect mobility in these materials. Experimental electrical conductivity results are useful in interpreting field measurements of the electrical response of the Earth and in estimating the temperature profile of the Earth based on conductivity-depth profiles derived from inversions of electromagnetic field results.

Grain boundaries are known to play an important role in many physical properties of rock including diffusion, creep, and electrical conduction. It has been previously suggested that grain boundaries may be responsible for enhanced conduction in olivine-rich rock (e.g., Shankland and Waff 1977; Shankland 1981; Kariya and Shankland 1983). A study by Schock et al. (1977) on the conductivity of ground-and-pressed polycrystalline olivine suggested that grain boundaries have only a small effect on the overall conductivity. The conductivity of a dunite from Jackson County, North Carolina has been studied by Constable and Duba (1990). They concluded that the grain boundaries do not enhance the conductivity of this rock and in fact they reported that the observed conductivity of the rock is lower than that of single crystal olivine under comparable conditions. Alternatively, Haak (1982) compared conductivity results of single and polycrystalline olivine samples and concluded that between 560 and 1150° C polycrystalline samples exhibit higher conductivity than single crystal samples. Because of higher activation energies for the single crystal samples than for the polycrystalline samples, the conductivities are equal at approximately 1400° C. One possibility considered by Haak is that the increased conductivity in the polycrystalline samples is a result of enhanced grain boundary conductivity caused by an increased number of paths for ionic diffusion.

Frequency dependent electrical measurements have been used by a number of authors to separate the contributions of the bulk (grain interior) and the grain bound-

* *Present address*: Lawrence Livermore National Laboratory, P.O. Box 808, L 365 Livermore, CA 94551, USA

aries of polycrystalline materials to the overall electrical properties of the material (e.g., Bauerle 1969; Chu and Seitz 1978; Lilley and Strutt 1979; Verkerk et al. 1982b; Tanaka et al. 1987). Tyburczy and Roberts (1990) and Roberts and Tyburczy (1991) applied impedance spectroscopy to polycrystalline olivine compacts and a natural dunite sample from San Quintin, Baja California, Mexico. They determined that the grain interior and grain boundary mechanisms add in a series manner leading to increased resistance and decreased conductivity (at zero frequency) for a polycrystalline material compared to a single crystal sample. In this work we investigate the frequency dependent electrical properties of two dunites and a single crystal olivine. We have determined the separate grain interior conductivity σ_{gi} and grain boundary conductivity σ_{gb} as a function of oxygen fugacity (f_{O_2}) from 1000 to 1200° C. By observing how the electrical impedance of olivine changes with changing conditions of temperature and f_{O_2} we learn more about the conduction mechanisms in these materials and can better evaluate the role of grain boundaries on the total electrical properties of rocks occurring within the Earth. In the rocks of this study, the grain interior and grain boundary resistivities add in series, resulting in a more resistive sample (at 0 Hz) than the grain interiors considered separately. The grain boundaries do not enhance the conductivity of any of the samples studied here, even though they are more conductive than the grain interiors in some cases.

Nomenclature

Impedance is the total opposition to current flow in response to an AC signal and is a complex quantity, generally expressed as a magnitude and a phase ($|Z|$, ϕ), as a real component and an imaginary component (Z', Z''), or as a resistance and a capacitance (R, C). In rocks impedance normally contains both resistive and capacitive components. The complex impedance Z^* is given by

$$Z^* = Z' - jZ'' \tag{1}$$

where the asterisk denotes a complex quantity, a single prime indicates a real quantity, the double prime indicates an imaginary quantity, and j is $\sqrt{-1}$. The real and imaginary parts of the impedance are obtained from the measured quantities $|Z|$ and ϕ determined at a given frequency by

$$Z' = |Z| \cos \phi, \tag{2}$$
$$Z'' = |Z| \sin \phi. \tag{3}$$

The complex resistivity ρ^* is obtained by multiplying the impedance by the geometric factor gf, which is the area to thickness ratio of the sample. The complex conductivity ψ^* is obtained by the taking the inverse of ρ^*. The complex conductivity is also represented as

$$\psi^* = \sigma + j\omega\varepsilon', \tag{4}$$

where the conductivity $\sigma = \omega\varepsilon''$, ω is the angular frequency, and ε' and ε'' are the real and imaginary parts

of the dielectric permittivity. ε^* is related to the complex impedance through

$$\varepsilon^* = (j\omega C_0 Z^*)^{-1} \tag{5}$$

where C_0 is the capacitance of the empty cell ($C_0 = \varepsilon_0 A/l$). The relative permittivity κ^* is the dielectric permittivity divided by the permittivity of free space $\varepsilon_0 = 8.854 \times 10^{-12}$ F/m. The complex impedances reported in this work can be converted to permittivities with (5).

Experimental Procedures

Materials Studied and Sample Preparation

Two different natural dunite samples were examined. The first natural sample is a dunite from the San Quintin volcanic field in Baja California, Mexico (SQD; Basu 1977; Basu and Murthy 1977). The dunite contains approximately 95% olivine (Fo$_{90.5}$), 3% clinopyroxene and 2% spinel (Fig. 1). It is relatively fine-grained with an average grain size of 0.2–0.4 mm. This sample has no
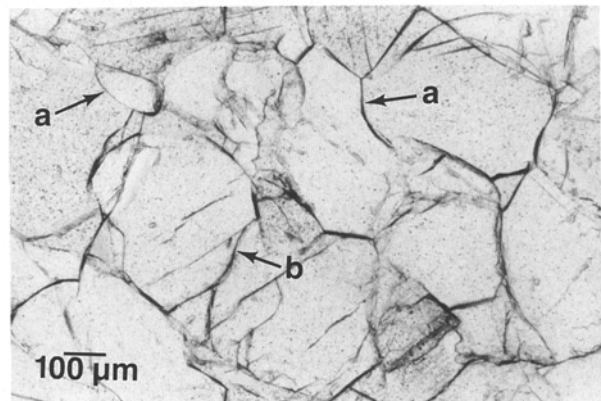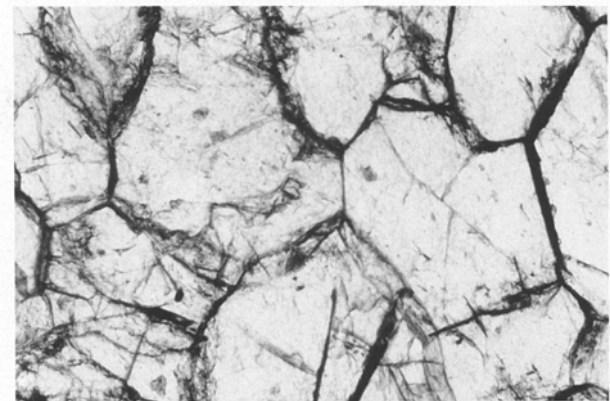

Fig. 1. Optical micrograph of San Quintin dunite, plane polarized light. The field of view consists entirely of olivine grains and shows little or no alteration along grain boundaries (a). The area indicated by (b) is a fracture across the large grain

North Carolina, plane, polarized light. The long dimension of the image is 1.5 mm. This material displays very little alteration along grain boundaries

serpentine or chlorite alteration and is an excellent rock for conductivity studies. The second natural dunite is from Jackson County, North Carolina (NCD; Fig. 2). It consists almost entirely of olivine ($Fo_{92.5}$) and has an average grain size of 0.4 mm. The Jackson County peridotite bodies have been partially serpentinized at their peripheries (Astwood et al. 1972). The samples used in this study were free of serpentine and chlorite phases as observed optically and with scanning electron microscopy (SEM), although in optical thin section, this rock does not have the clean, "tight" grain boundaries observed in the SQD. Because of the differences in Fe content and visible character of the grain boundaries, it is useful to compare the electrical properties of these rocks.

Single crystal samples were prepared from large gem quality specimens from San Carlos, Arizona (Fo_{91}; SC). These specimens were oriented optically to within $\pm 3°$ to the [001] axis. The specimens selected for study were carefully examined optically to $500 \times$ to insure that they were free of fractures and inclusions.

Electrical measurements were made on disks that were polished on both sides using diamond paste with a final grit of 0.25 μm. The samples were cleansed and rinsed ultrasonically in ethanol prior to applying electrodes. The two-electrode technique was generally used for the electrical measurements, except for specific cases in which four-electrode methods were used. Electrodes were either sputtered Pt followed by Pt paint and a thin Pt sheet, Pt paint and Pt sheet, or sputtered Pt and Ir sheet. The thickness of sputtered coatings was between 200 and 300 Å. Both painted and sputtered electrodes give satisfactory results. One problem that results from using Pt and Ir electrodes is the loss of Fe from the sample to the electrodes. Samples were checked with the electron microprobe for Fe loss after each experimental run. The loss of Fe was confined to the outermost 25 μm of the sample (or less) and the loss in this outer zone was generally less than 2 wt% Fe. One effect of Fe loss is the increase of Z' over the entire frequency range. Iron loss was checked for during the experiments by making measurements at a specific frequency (typically 100 Hz) at different times during the course of an experiment. Over the course of an experiment, usually 10 to 24 hours, the variation in Z' and $|Z|$ after equilibration was generally less than 5%. Hirsch and Shankland (1991b) present a quantitative model of electrical conduction in olivine and determine that a small loss of Fe to electrodes does not significantly affect electrical conductivity and oxygen diffusivity in olivine.

The electrical measurements were made in a one atmosphere total pressure gas mixing furnace. Samples were placed into the furnace and allowed to equilibrate to experimental conditions for a period of 4–20 hours. The length of time required for the sample to equilibrate is related to the sample dimensions, grain size, experimental temperature, and the mobility of point defects. During equilibration the resistance of the sample was monitored at specific frequencies and gradually reached a steady value. The oxygen fugacity was controlled with a CO/CO_2 mixture and was accurate to within ± 0.15 log units checked with an yttria-stabilized zirconia oxy-

gen sensor. Temperatures were controlled and monitored to $\pm 3°$ C with type B Pt 70-Rh 30/Pt 94-Rh 6 thermocouples. The temperature gradient between the top and bottom of the sample was less than 1° C.

Impedance Measurements

Electrical measurements were made over the frequency range 5×10^{-5} to 10^5 Hz using two data collection systems. Between 5×10^{-5} and 10^4 Hz data was collected using the system described previously by Roberts and Tyburczy (1991) that was designed after the system de-
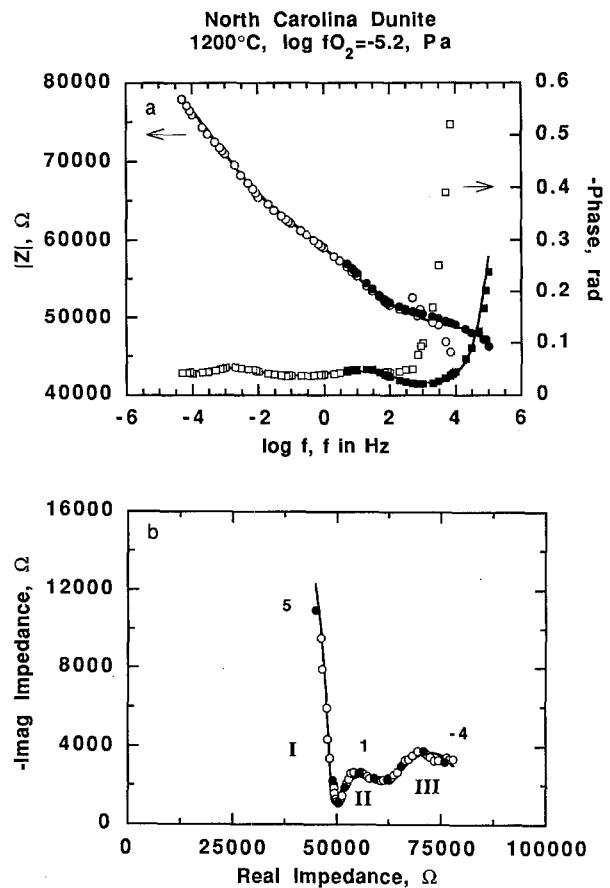

Fig. 3a, b Impedance data for the North Carolina Dunite collected at 1200° C and an f_{O_2} of $10^{-5.2}$ Pa. **a** Impedance magnitude and phase angle versus log frequency in Hz. All data collected by both the high frequency (HF) and low frequency (LF) systems are displayed. Symbols: open circles, $|Z|$, LF; solid circles, $|Z|$, HF; open squares, phase angle, LF; solid squares, phase, HF. The two systems are in good agreement over the frequency range 5 to 100 Hz, and depart significantly above 1000 Hz as a result of system capacitance in the low frequency measuring system. The crossover frequency is the frequency at which we have combined data sets, and is usually between 30 and 70 Hz. In this experiment the crossover frequency is 50 Hz. **b** The complex impedance plane plot of the data displays three impedance arcs, referred to as arcs I, II, and III from high to low frequency as indicated on the diagram. A filled circle occurs every decade of frequency; numerals are log frequency of the corresponding filled data point. The impedance arcs can be incomplete if they extend past the range of frequency measurement. The lines through the data are model responses obtained from CNLS fitting with an equivalent circuit

scribed in detail by Olhoeft (1979, 1985). At frequencies from 5 to 10^5 Hz, data was collected with a Hewlett Packard 4192 Impedance Spectrum Analyzer. At each frequency the measured parameters are the impedance magnitude and phase. The two systems overlap in frequency from 5 Hz to 10 kHz (Figure 3 a, b). In the frequency range 5–100 Hz measurements of $|Z|$ and ϕ are nearly identical for the two systems. The low frequency system is limited at high frequencies because of cross-talk between the leads and the frequency response of the instrumentation amplifiers. The high frequency system has a built in correction to eliminate the effects of stray capacitance at the highest frequencies. The cross-over frequency band, at which we have combined data sets for input into CNLS analysis, is typically 30–70 Hz. Accuracy of the measuring systems was checked by analyzing RC circuits of resistors and capacitors with values known to within 1%. Numerous tests were performed using components with a range of values approximating those of the experiments. The accuracy of the measured parameters $|Z|$ and ϕ was within the tolerance of the known standards.

Experimental Data

The impedance measurements shown in Fig. 3 are typical of the electrical response observed for the natural dunite. The data shown in this figure are the results of an experiment on the NCD performed at a temperature of 1200° C, and an f_{O_2} of 6.31×10^{-6} Pa. Figure 3 a displays the measured parameters $|Z|$ and ϕ plotted against log frequency. The phase angle displays a strong dependence on frequency and two relative minima (phase angle nearest zero) are clearly seen. The impedance magnitude increases with increasing frequency across the entire frequency spectrum, but the increase is not linear with log frequency. In Fig. 3 b, the imaginary part of the complex impedance Z'' is plotted against the real part Z', in what is referred to as a 'complex plane' plot. The complex impedance plane plot displays parts of three impedance arcs, which are sub-circular arcs approximately centered on the real axis. Each arc corresponds to a separate conduction process or mechanism that is dominant at a different range of frequency and has a different relaxation time τ relative to the other arcs. In general, each experiment displays two or three impedance arcs occurring at high, intermediate, and low frequency ranges (referred to as arcs I, II, and III, respectively, Fig. 3 b). An arc can be partial or incomplete if it extends past the range of measurement and adjacent impedance arcs can overlap.

The interpretation of the mechanism causing each arc is grain interior conduction at the highest frequency range, grain boundary conduction at intermediate frequencies, and electrode-sample response at the lowest frequencies. This interpretation is based on comparison of single and polycrystalline experiments, experiments on polycrystalline sample with varying dimensions, and experiments utilizing different electrode configurations (Tyburczy and Roberts 1990; Roberts and Tyburczy

1991, 1992 a). Numerous other polycrystalline materials display a similar type of electrical response including $ZrO_2 \cdot Y_2O_3$ (Bauerle 1969), Al_2O_3 (Lilley and Strutt 1979), $BaTiO_3$ (Chiou et al. 1989), and $CeO_2 \cdot Y_2O_3$ (Gerhardt and Nowick 1986).

Modeling the Data with Equivalent Circuits

Each experimental impedance spectrum is modeled using a circuit of resistors and capacitors. A complex non-linear least squares (CNLS) fitting routine is used to get the best fit. By fitting the data in this way, values for individual resistors and capacitors are obtained that are then related to specific conduction and polarization mechanisms within the material (Macdonald 1985; Roberts and Tyburczy 1991). Because we observe impedance arcs that have different time constants, i.e., the impedance arcs occur over different ranges of frequency and are separate on complex impedance plane plots, the equivalent circuit generally consists of two or more parallel RC circuit elements connected in series.

A parallel RC element produces a semi-circle in the complex impedance plane, having a center that falls on the real axis. The complex impedance of a parallel RC circuit is given by

$$Z^* = \frac{R - j\omega C R^2}{1 + \omega^2 C^2 R^2}. \tag{6}$$

As $\omega \to 0$, the impedance is equal to the resistor value R, or the width of the impedance arc, and there is no capacitive component. Because in real materials the electrical response often exhibits impedance arcs with centers that lie below the real axis, a distributed element (CPE) is used in the equivalent circuit to empirically describe
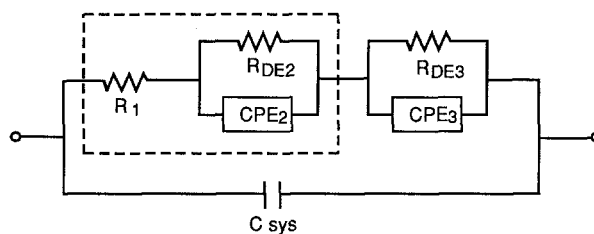

Fig. 4. The general form of the equivalent circuit used to model the overall response observed in the samples of this study. This circuit produces three impedance arcs in the complex plane, two of which can have centers below the real axis, appropriate for the polycrystalline samples. R_1 corresponds to the grain interior resistance, R_{DE2} and CPE_2 correspond to grain boundary properties, and R_3 and CPE_3 relate to electrode properties. If only two impedance arcs are observed as in the single crystal experiments, one distributed element (R_{DE2}, CPE_2) is removed from the circuit. The portion of the circuit enclosed by the dashed box indicates the parts of the circuit that correspond solely to properties of the material. The system capacitance C_{sys} is in parallel with the entire circuit. Use of the high frequency measuring system, which has a much lower C_{sys} than the low frequency measuring system, enables a reasonable estimate of the grain interior capacitance (not shown)

Table 1. Experimental conditions and parameters derived from fits to the data using the equivalent circuit of Fig. 4

Sample	Temp (°C)	$\log f_{O_2}$ (Pa)	Geometric factor (m)	R_1 (Ω)	C_1 (pF)	R_{DE2} (Ω)	τ_{DE2} (s)	α_{DE2}	R_{DE3} (Ω)	τ_{DE3} (s)	α_{DE3}
NCD1E	1004	−12.0	0.041	$3.45 \pm 0.08 \times 10^5$	$2.70 \pm 0.03 \times 10^{-10}$	$8.43 \pm 0.90 \times 10^4$	$2.16 \pm 0.93 \times 10^{-2}$	0.35 ± 0.04	n.d.	n.d.	n.d.
NCD1D	1004	−9.54		$2.91 \pm 0.15 \times 10^5$	$2.71 \pm 0.03 \times 10^{-10}$	$2.83 \pm 0.21 \times 10^5$	$2.11 \pm 0.99 \times 10^{-1}$	0.19 ± 0.02	n.d.	n.d.	n.d.
NCD1C	1004	−7.93		$2.94 \pm 0.06 \times 10^5$	$2.64 \pm 0.02 \times 10^{-10}$	$3.11 \pm 0.09 \times 10^5$	$3.00 \pm 0.49 \times 10^{-1}$	0.32 ± 0.01	n.d.	n.d.	n.d.
NCD1F	1004	−7.93		$2.61 \pm 0.09 \times 10^5$	$2.58 \pm 0.02 \times 10^{-10}$	$2.46 \pm 0.11 \times 10^5$	$8.73 \pm 2.69 \times 10^{-1}$	0.18 ± 0.01	n.d.	n.d.	n.d.
NCD1G	1004	−6.13		$2.03 \pm 0.05 \times 10^5$	$2.67 \pm 0.02 \times 10^{-10}$	$2.33 \pm 0.10 \times 10^5$	$2.27 \pm 0.50 \times 10^0$	0.22 ± 0.01	n.d.	n.d.	n.d.
NCD1H	1004	−5.20		$1.55 \pm 0.04 \times 10^5$	$2.80 \pm 0.05 \times 10^{-10}$	$2.48 \pm 0.11 \times 10^5$	$5.77 \pm 1.46 \times 10^0$	0.24 ± 0.01	n.d.	n.d.	n.d.
NCD2B	1101	−8.06	0.0553	$1.28 \pm 0.02 \times 10^5$	$7.79 \pm 0.16 \times 10^{-12}$	$2.14 \pm 1.03 \times 10^4$	$3.47 \pm 1.01 \times 10^{-3}$	0.30 ± 0.05	$9.97 \pm 14.9 \times 10^4$	$5.56 \pm 73.9 \times 10^6$	0.15 ± 0.11
NCD2C	1101	−6.56		$1.15 \pm 0.01 \times 10^5$	$7.77 \pm 0.04 \times 10^{-12}$	$2.17 \pm 0.25 \times 10^4$	$9.72 \pm 2.02 \times 10^{-3}$	0.38 ± 0.02	$4.92 \pm 0.97 \times 10^4$	$2.44 \pm 1.89 \times 10^3$	0.27 ± 0.04
NCD2D	1101	−6.00		$1.04 \pm 0.02 \times 10^5$	$7.52 \pm 0.05 \times 10^{-12}$	$2.69 \pm 0.11 \times 10^4$	$2.02 \pm 0.26 \times 10^{-2}$	0.38 ± 0.01	$3.99 \pm 0.24 \times 10^4$	$1.14 \pm 0.16 \times 10^3$	0.38 ± 0.02
NCD2A	1101	−5.82		$1.02 \pm 0.03 \times 10^5$	$8.51 \pm 0.08 \times 10^{-12}$	$2.19 \pm 0.14 \times 10^4$	$9.28 \pm 1.69 \times 10^{-3}$	0.39 ± 0.02	$3.26 \pm 0.27 \times 10^4$	$5.06 \pm 0.94 \times 10^2$	0.38 ± 0.03
NCD2E	1101	−5.20		$8.84 \pm 0.01 \times 10^4$	$8.15 \pm 0.05 \times 10^{-12}$	$2.77 \pm 0.09 \times 10^4$	$3.79 \pm 0.33 \times 10^{-2}$	0.45 ± 0.01	$4.26 \pm 0.22 \times 10^4$	$5.10 \pm 0.59 \times 10^2$	0.40 ± 0.02
NCD2F	1101	−4.40		$6.35 \pm 0.01 \times 10^4$	$8.69 \pm 0.10 \times 10^{-12}$	$2.73 \pm 0.11 \times 10^4$	$4.92 \pm 0.45 \times 10^{-2}$	0.50 ± 0.01	$4.52 \pm 0.21 \times 10^4$	$2.35 \pm 0.20 \times 10^2$	0.41 ± 0.02
NCD3D	1200	−8.06	0.0553	$7.14 \pm 0.07 \times 10^4$	$7.99 \pm 0.16 \times 10^{-12}$	$7.87 \pm 0.67 \times 10^3$	$6.42 \pm 0.33 \times 10^{-3}$	0.59 ± 0.03	$7.09 \pm 1.52 \times 10^4$	$1.87 \pm 4.43 \times 10^6$	0.14 ± 0.02
NCD3C	1200	−6.56		$5.66 \pm 0.08 \times 10^4$	$8.47 \pm 0.21 \times 10^{-12}$	$3.39 \pm 0.27 \times 10^3$	$1.06 \pm 0.08 \times 10^{-2}$	0.83 ± 0.05	$8.52 \pm 1.22 \times 10^4$	$1.71 \pm 4.00 \times 10^6$	0.10 ± 0.01
NCD3B	1200	−5.20		$4.80 \pm 0.01 \times 10^4$	$8.89 \pm 0.30 \times 10^{-12}$	$1.38 \pm 0.11 \times 10^4$	$1.69 \pm 0.39 \times 10^{-2}$	0.39 ± 0.02	$2.27 \pm 0.18 \times 10^4$	$3.71 \pm 0.60 \times 10^2$	0.38 ± 0.03
NCD3A	1200	−4.36		$3.80 \pm 0.01 \times 10^4$	$9.67 \pm 0.24 \times 10^{-12}$	$1.11 \pm 0.04 \times 10^4$	$1.16 \pm 0.13 \times 10^{-2}$	0.42 ± 0.01	$1.74 \pm 0.07 \times 10^4$	$1.04 \pm 0.08 \times 10^2$	0.57 ± 0.02
NCD3E	1200	−3.07		$2.69 \pm 0.02 \times 10^4$	$9.64 \pm 0.26 \times 10^{-12}$	$1.38 \pm 0.05 \times 10^4$	$2.54 \pm 0.21 \times 10^{-2}$	0.56 ± 0.01	$3.21 \pm 0.08 \times 10^4$	$1.29 \pm 0.08 \times 10^2$	0.45 ± 0.01
SQD5E[1]	1200	−8.06	0.0289	$7.76 \pm 0.24 \times 10^4$	$9.17 \pm 0.84 \times 10^{-11}$	$1.07 \pm 0.03 \times 10^5$	$1.11 \pm 0.16 \times 10^0$	0.30 ± 0.01	*	*	*
SQD5D	1200	−6.56		$7.43 \pm 0.23 \times 10^4$	$1.11 \pm 0.10 \times 10^{-10}$	$1.17 \pm 0.03 \times 10^5$	$2.67 \pm 0.40 \times 10^0$	0.30 ± 0.01	*	*	*
SQD5A	1200	−4.28		$5.21 \pm 0.06 \times 10^4$	$9.42 \pm 0.31 \times 10^{-12}$	$9.48 \pm 0.09 \times 10^4$	$4.72 \pm 0.22 \times 10^0$	0.36 ± 0.01	*	*	*
SQD5C	1200	−4.28		$5.80 \pm 0.16 \times 10^4$	$8.76 \pm 0.72 \times 10^{-12}$	$1.13 \pm 0.03 \times 10^5$	$4.77 \pm 0.62 \times 10^0$	0.33 ± 0.01	*	*	*
SQD5B	1200	−3.06		$4.81 \pm 0.10 \times 10^4$	$8.78 \pm 0.44 \times 10^{-12}$	$1.01 \pm 0.01 \times 10^5$	$3.58 \pm 0.22 \times 10^0$	0.35 ± 0.01	*	*	*
SC19A	1001	−7.93	0.0257	$1.49 \pm 0.02 \times 10^5$	$2.79 \pm 0.05 \times 10^{-10}$	$3.16 \pm 0.03 \times 10^5$	$1.18 \pm 0.04 \times 10^{-1}$	0.48 ± 0.01	*	*	*
SC19B	1001	−6.13		$1.22 \pm 0.22 \times 10^5$	$2.68 \pm 0.05 \times 10^{-10}$	$5.80 \pm 0.06 \times 10^5$	$1.12 \pm 0.03 \times 10^0$	0.54 ± 0.01	*	*	*
SC19C	1001	−5.20		$5.87 \pm 0.05 \times 10^4$	$2.71 \pm 0.06 \times 10^{-10}$	$9.16 \pm 0.11 \times 10^5$	$4.53 \pm 0.18 \times 10^0$	0.59 ± 0.04	*	*	*

NCD, North Carolina dunite; SQD, San Quintin dunite; SC19, San Carlos olivine single crystal [001]. Geometric factor (gf) is the area/length ratio of the experimental cell. 1) The 4-electrode method was used on the San Quintin samples. n.d. – not determined. * – no impedance arc
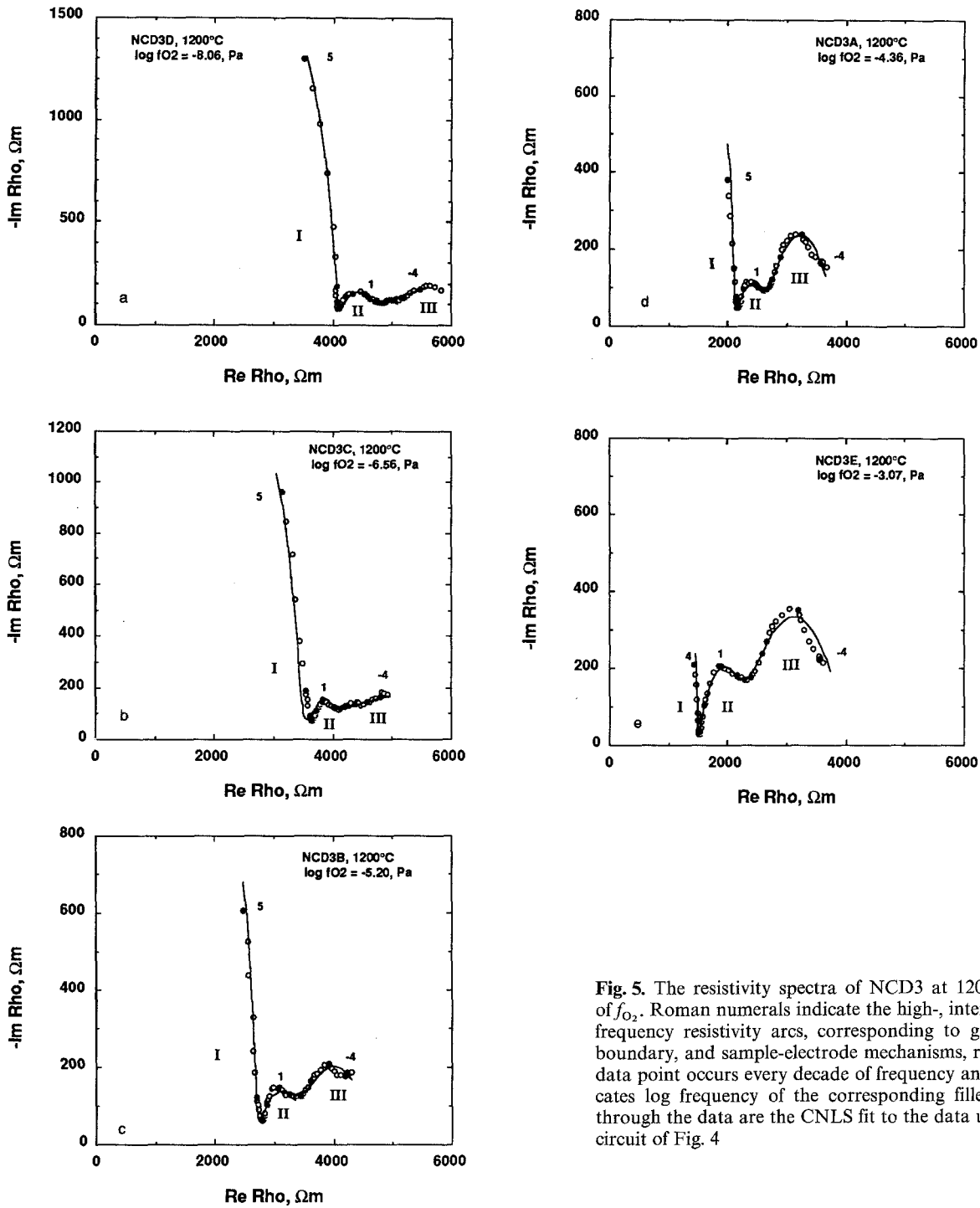
Fig. 5. The resistivity spectra of NCD3 at 1200° C as a function of f_{O_2}. Roman numerals indicate the high-, intermediate-, and low-frequency resistivity arcs, corresponding to grain interior, grain boundary, and sample-electrode mechanisms, respectively. A filled data point occurs every decade of frequency and the numeral indicates log frequency of the corresponding filled point. The lines through the data are the CNLS fit to the data using the equivalent circuit of Fig. 4

the depressed impedance arcs. The equation that describes the response of a CPE in parallel with a resistor is

$$Z^*_{ZARC} = \frac{R}{1 + (j\omega\tau)^\alpha} \qquad (7)$$

where Z^*_{ZARC} indicates the complex impedance of an arc depressed in the impedance plane. The exponent α relates to θ the angle of depression of the impedance arc $(\alpha = 1 - 2\theta/\pi)$ and varies between 0 and 1. For $\alpha = 1$ the

CPE is an ideal capacitor (no depression, center of impedance arc falls on the real axis) and there is a single time constant τ equal to $R \cdot C$. For $\alpha = 0$ the CPE is an ideal resistor and there is no imaginary (capacitive) component. Distributed elements and their responses are discussed by many authors (e.g., Macdonald 1985; Raistrick 1987). The general form of the equivalent circuit used to model the results of this study is shown in Fig. 4. When only two impedance arcs are observed the equivalent circuit is modified by removing either the second element (grain boundaries in the single crystal case), or
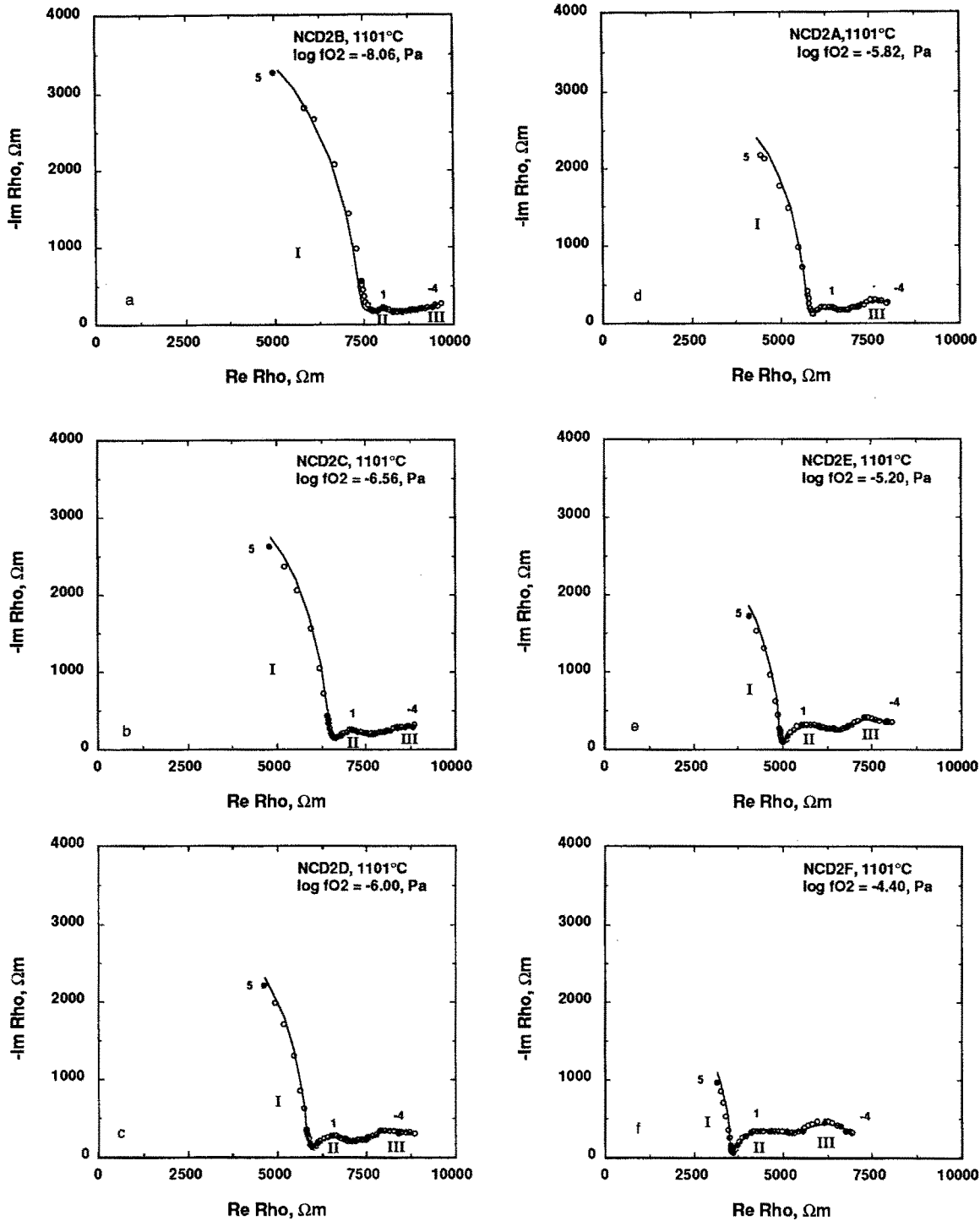
Fig. 6. The resistivity spectra of NCD2 at 1101° C as a function of f_{O_2}. Roman numerals indicate the high-, intermediate-, and low-frequency resistivity arcs, corresponding to grain interior, grain boundary, and sample-electrode mechanisms, respectively. A filled data point occurs every decade of frequency and the numeral indicates log frequency of the corresponding filled point. The lines through the data are the CNLS fit to the data using the equivalent circuit of Fig. 4

the third element (electrode response in the polycrystalline sample, four-electrode configuration).

Using the circuit in Fig. 4 and a CNLS fitting routine (Macdonald et al. 1982; Hurt and Macdonald 1986) we were able to fit the data and obtain values for each of the specific components and parameters. Models of the data obtained in this manner are shown as lines through

the experimental data for each experiment. The circuit parameters obtained from the CNLS fit for each experiment are listed in Table 1, along with the estimated standard deviations for each parameter. The resistances, resistivities, and conductivities obtained from the parameters in Table 1 are DC values for the corresponding conduction mechanism. The parameters for the third circuit

element are not always determined. The two reasons for this are 1) only two impedance arcs are observed in the impedance spectrum, as is the case in the single crystal and four-electrode experiments, and 2) there were not enough data points describing the electrode arc for an adequate fit to be obtained.

Results

Impedance Spectra

Effect of Oxygen Fugacity on Impedance Spectra. The resistivity spectra (impedance spectra corrected for sample dimensions) for NCD3 (1200° C) are shown in Fig. 5 as a function of increasing f_{O_2}. The approximate stability field of Fo_{90} at 1200° C is between f_{O_2}'s of $10^{-8.88}$ to $10^{0.63}$ Pa (Nitsan 1974). At the highest f_{O_2}'s of our experiments, three resistivity arcs are clearly observed. At the lowest f_{O_2}'s the low frequency portion of the spectrum is not well resolved; the grain boundary arc in particular is very small compared to the grain interior arc. As the f_{O_2} increases, the grain boundary arc emerges and becomes more distinct while the grain interior arc decreases in width. These changes in the resistivity spectra indicate that the grain interiors become more conductive with increasing f_{O_2}, while the grain boundaries become more resistive with increasing f_{O_2}. Similar changes are also seen in the resistivity spectra of NCD2 (1101° C, Fig. 6).

The resistivity spectra of the San Quintin dunite at 1200° C and a range of f_{O_2} from $10^{-8.06}$ to $10^{-3.06}$ Pa are shown in Fig. 7. The four-electrode technique was used to measure the impedance of these samples and no electrode response appears in these spectra. The general electrical response of the SQD is similar to that of the NCD in that two impedance arcs related to prop-
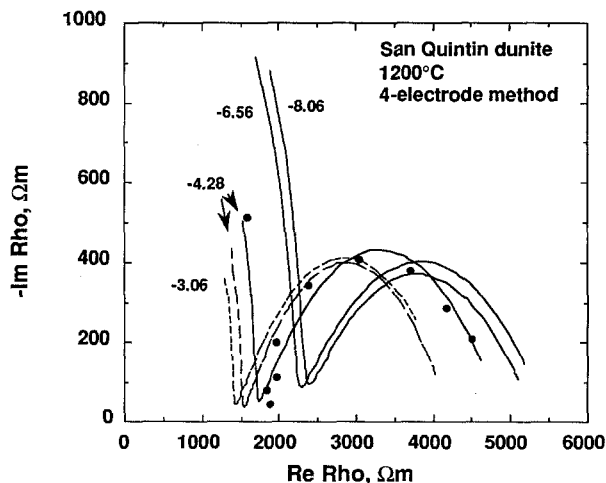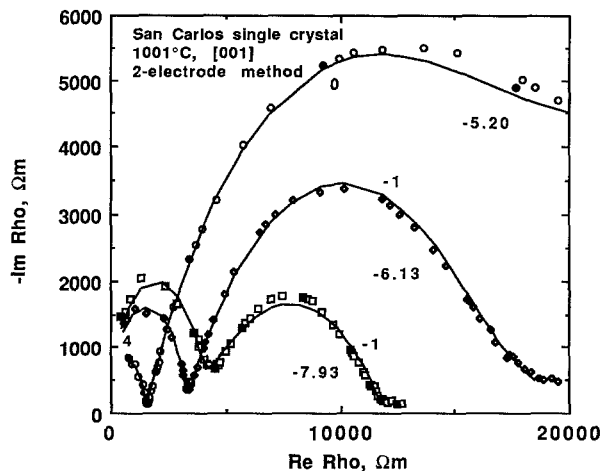

Fig. 8. The resistivity spectra of SC19 at 1000 °C as a function of f_{O_2}. A filled data point occurs every decade of frequency and the numeral indicates log frequency of the corresponding filled point. The highest frequency reported for each curve is 10^4 Hz. The spectra shown were taken at f_{O_2}'s of $10^{-7.93}$, $10^{-6.13}$, and $10^{-5.20}$ Pa, as indicated on the diagram. The lines through the data are the CNLS fit to the data using the equivalent circuit of Fig. 4, modified to produce only two impedance arcs. Only data taken using the low-frequency measuring system are reported for these experiments

erties of the material are present. The grain interior mechanism decreases in resistivity with increasing f_{O_2}, however, there is very little variation in the width of the grain boundary arc with changes in f_{O_2}.

We have measured the impedance of a San Carlos olivine single crystal in the [001] direction at 1001° C at f_{O_2}'s of $10^{-7.93}$, $10^{-6.13}$, and $10^{-5.20}$ Pa (Fig. 8). The resistivity spectra of the single crystal displays two arcs, one at high frequency corresponding to conduction in the crystal, and one at lower frequencies related to electrode effects. The grain interior arc width decreases with increasing f_{O_2}, and the electrode response arc width increases with increasing f_{O_2}. The electrode arc at the highest f_{O_2} is no longer semicircular, but becomes asymmetric at the lowest frequencies. One possible reason for the changes in the electrode arc with changing f_{O_2} is the decreased activity of Fe in Pt at higher f_{O_2}'s (Gudmundsson et al. 1992). The decreased Fe activity may cause the electrodes to be more blocking to charge carriers at the highest f_{O_2}'s.

A similar, but less pronounced, electrode response is observed in the NCD spectra (Fig. 5). The spectra of NCD1 (1004° C; Fig. 9) display a greater amount of scatter than the other NCD spectra. This is particularly true for the low frequency portion of each spectrum (<10 Hz). The low frequency impedance arcs are not well-resolved and it was difficult to obtain fit parameters for the grain boundary and electrode mechanisms. One reason for this is that the measured impedances at 1004° C and low frequency are commonly greater than 500 kΩ. The measurements are more susceptible to noise and electrical interference at high impedance values. At an f_{O_2} of 10^{-12} Pa (Fig. 9a) there is only one well-defined impedance arc; that being the one corresponding to

Fig. 7. The modeled resistivity spectra of SQD5 at 1200° C as a function of f_{O_2}. The four-electrode configuration was used in these experiments, hence they lack a response due to the sample-electrode interface. The numbers represent log f_{O_2} (Pa) of the corresponding model curve. The *solid circles* are data points for the experiment performed at an f_{O_2} of $10^{-4.28}$ Pa (*solid line*), one point is reported per decade frequency
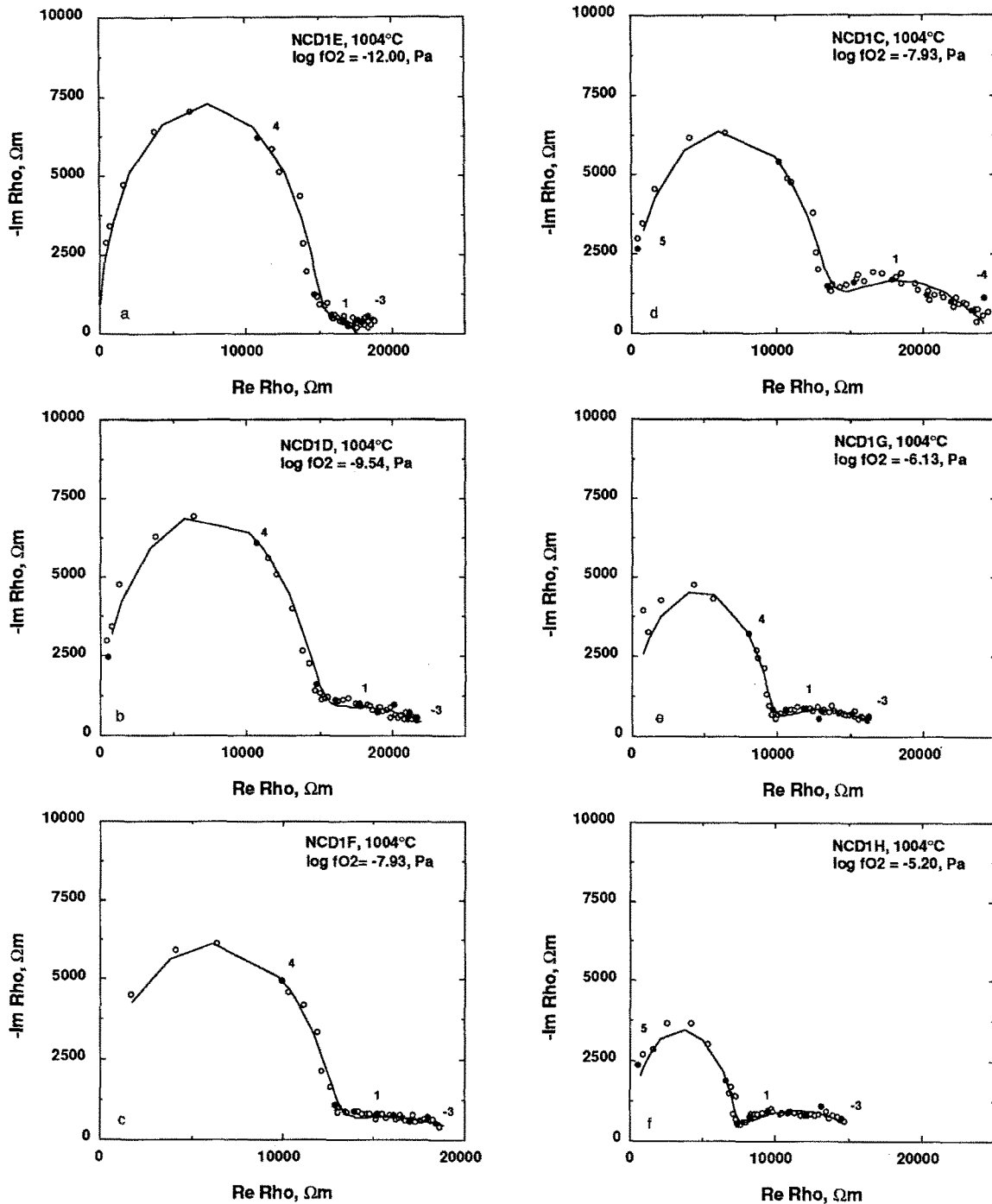
Fig. 9. The resistivity spectra of NCD1 at 1004° C as a function of f_{O_2}. A filled data point occurs every decade of frequency and the numeral indicates log frequency of the corresponding filled point. The lines through the data are the CNLS fit to the data using the equivalent circuit of Fig. 4. Only data taken using the low-frequency measuring system are reported for these experiments. The inflated high-frequency impedance arc is a consequence of the increased system capacitance of the low-frequency measuring system

grain interiors. The low impedance portion of this spectrum is poor and cannot be fit properly. At higher f_{O_2}'s some of the spectra display two overlapping arcs at frequencies lower than that of the grain interior response. Two experiments run at the same f_{O_2} (Fig. 9c, d) display very similar grain interior arcs with slightly different responses at low frequency. The low frequency portions of NCD spectra at higher temperatures are much more

well-defined. It is unclear why single crystal olivine at 1001° C produces a pronounced electrode arc, while the NCD at 1004° C does not.

Because of the difficulty in CNLS fitting of NCD1 and the ambiguity in the number of impedance arcs of this experiment at low frequency, only the high frequency grain interior fit parameters of this experiment (Table 1; R_1, C_1) can be used with confidence. Additional work

needs to be performed to understand the differences between the single and polycrystalline electrode response and the polarization mechanisms at the sample-electrode interface.

Conductivity Results and Comparison to Other Studies

The conductivity of each experiment ($\sigma = 1/\rho$) has been calculated from the resistances and sample dimensions listed in Table 1. Conductivities obtained in this manner are DC conductivities of the respective conduction mechanism. The conductivities and resistivities of the grain boundaries are given as macroscopic properties, that is, the resistance is corrected for the overall sample dimensions, not the actual volume of the grain boundary phase itself ($\rho_{gb} = R_{gb} A/l$ and $\sigma_{gb} = (1/R_{gb}) \cdot l/A$). Determined in this manner, ρ_{gb} and σ_{gb} are the normalized resistance and conductance. All grain boundary resistivities and conductivities reported here are macroscopic properties unless otherwise designated. Additional discussion of macroscopic and microscopic grain boundary electrical properties follows in the Discussion section. The log of the conductivity of the grain interiors, grain boundaries, and the series total of the grain interior and grain boundary conductivities is plotted as a function of $\log f_{O_2}$ in Fig. 10 for the North Carolina dunite at 1200° C. The general response of the grain interiors is typical for all the experiments in this study; conductivity and slope increase with increasing f_{O_2}. For all the experiments the slope of the grain interiors at the highest f_{O_2}'s is between 1/9 and 1/5. One interesting result is that the grain boundaries of NCD2 and NCD3 display a negative f_{O_2} dependence. Because the grain interior and grain boundary resistivity mechanisms add in series, the total conductivity is lower than either mechanism considered separately. That is, $\rho_{total} = \rho_{gi} + \rho_{gb}$, and $\sigma_{total} = (1/\sigma_{gi} + 1/\sigma_{gb})^{-1}$. This situation occurs despite the grain boundaries being more conductive than the grain interiors. At 1200° C the grain boundaries contribute very

little to the total conductivity at the lowest f_{O_2}'s, and have a greater contribution to σ_{total} as f_{O_2} increases. Series behavior is also observed in polycrystalline olivine compacts (Tyburczy and Roberts 1990; Roberts and Tyburczy 1991).

Also shown on Fig. 10 is the conductivity data from Constable and Duba (1990). Their measurements were performed on a dunite from Jackson County, North Carolina, a rock similar to the Jackson County dunite used in the present study, but it may not be from precisely the same location. In Constable and Duba's study, the conductivity was determined by making measurements over the frequency range 0.1–10 kHz and they report little or no dependence of conductivity on frequency. This frequency range roughly corresponds to the high frequency grain interior mechanism. The agreement between the two results is quite good, with the data from Constable and Duba about 0.2 log units lower in conductivity than in our determination over the entire range of f_{O_2} measured. The similarity in the two results is an encouraging indication of inter-laboratory agreement.

As a comparison, σ_{gi}, σ_{gb}, and σ_{total} at 1200° C for the San Quintin dunite are plotted against $\log f_{O_2}$ in Fig. 11. The grain interiors of SQD are more conductive than those of NCD over the entire range of f_{O_2}. This is probably a result of the higher Fe content in the SQD. Again, σ_{gi} displays a gradual increase in conductivity and slope with increasing f_{O_2}. A significant difference between the two dunites at 1200° C is in the grain boundary conductivity. The grain boundary conductivity of SQD shows little or no f_{O_2} dependence and is lower in conductivity than the grain interior mechanism. The result is that the SQD is a less conductive rock than the NCD, even though the SQD is richer in Fe. In both rocks the grain boundaries do not enhance the conductivity of the material, but over certain ranges of f_{O_2} play an important role in determining the total conductivity. These differences demonstrate the variability of grain boundary properties in natural rocks. The SQD shows very tight, "clean" grain boundaries in thin section and
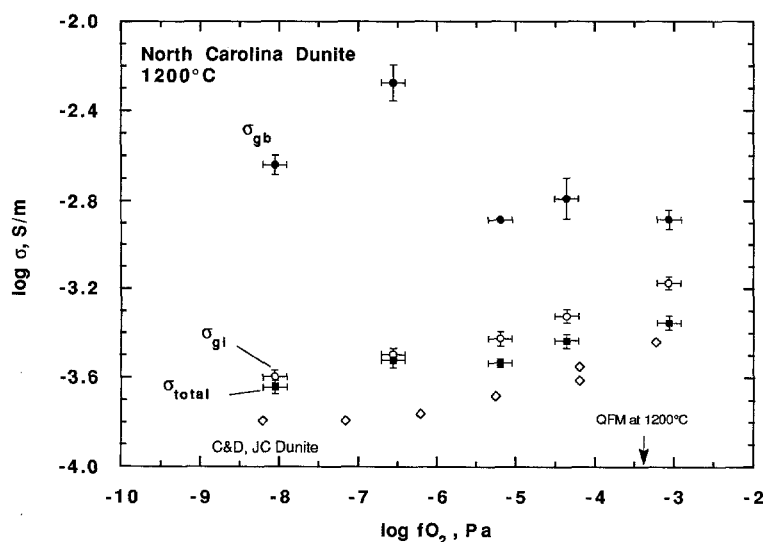

Fig. 10. Log σ as a function of $\log f_{O_2}$ for NCD3 at 1200° C. For this rock, $\sigma_{gb} > \sigma_{gi}$ over the entire range of f_{O_2}. At the lowest f_{O_2}'s the grain boundaries affect σ_{total} very little, and have the greatest influence at the highest f_{O_2}'s (compare to the San Quintin dunite at 1200° C, Fig. 11). The grain boundary conductivities display a negative f_{O_2} dependence. Diamonds are the conductivity of Jackson County, North Carolina dunite as determined by Constable and Duba (1990) at frequencies between 0.1 and 10 kHz (1200° C). Their experiments display an f_{O_2} dependence similar to that of the grain interior conductivity of NCD3 of this work, with about a 0.2 log σ offset over the entire range of f_{O_2}. The arrow indicates the f_{O_2} of the QFM buffer assemblage at 1200° C
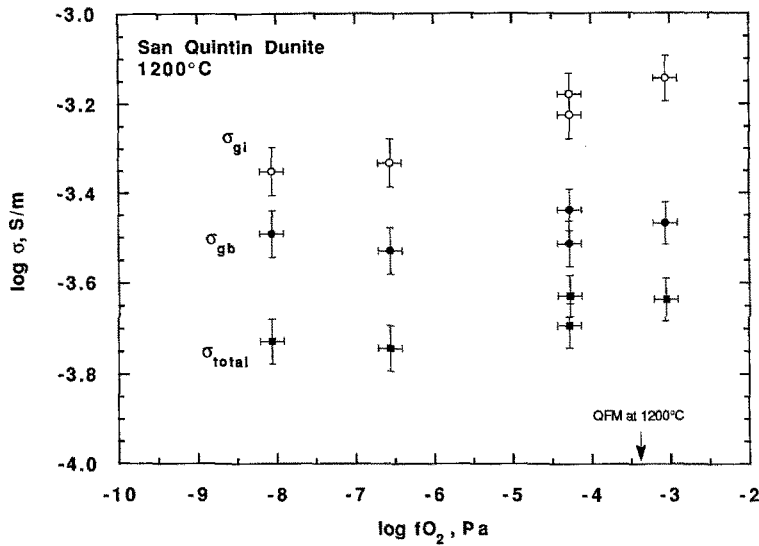
Fig. 11. Log σ as a function of $\log f_{O_2}$ for the SQD5 at 1200° C. This rock displays grain boundaries that are more resistive than grain interiors over entire range of f_{O_2}, and the grain boundary conductivities are nearly independent of f_{O_2}. At the highest f_{O_2}'s σ_{total} is dominated by the more resistive grain boundaries, in contrast to NCD3 (Fig. 10). The arrow indicates the f_{O_2} of the QFM buffer assemblage at 1200° C
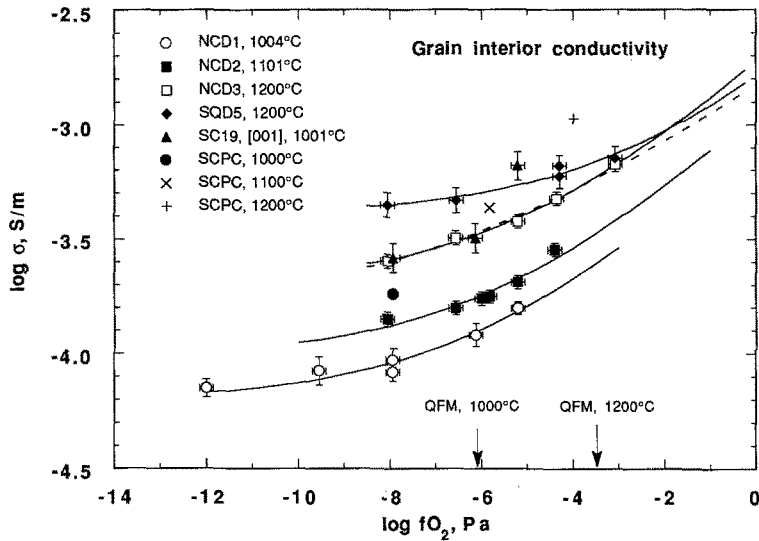

Fig. 12. Log σ_{gi} versus $\log f_{O_2}$ for all the experiments, including the San Carlos single crystal and San Carlos polycrystalline compacts (SCPC; Roberts and Tyburczy 1991). Lines are fits to the data using (8) in the text. These fits assume an exponential f_{O_2} dependence of $1/5.5$. The dashed line fit to the 1200° C NCD data assumes an exponential f_{O_2} dependence of $1/7$ for comparison. Both exponents provide adequate fits to the data over the range of f_{O_2} of the experiments. The fit parameters are listed in Table 2

SEM. The grain boundaries in the NCD have a different appearance, although no weathering products are observed in pre-run optical and post-run SEM inspections (see Figs. 1, 2). Physical differences in the grain boundaries (structure and/or composition) are possible reasons for the differences in σ_{gb} between the two rocks.

Grain Interior Conductivity. The grain interior conductivities for all the experiments performed are plotted as a function of f_{O_2} in Fig. 12. The single crystal results for San Carlos single crystal olivine (SC19) are also shown on this diagram (1000° C, [001] orientation). The SC19 conductivities display a positive f_{O_2} dependence that is steeper than the polycrystalline results. The SC19 conductivities are also higher than the grain interior conductivities of the NCD. This relationship can be partly attributed to taking measurements in the most conductive crystallographic direction and partly to greater Fe content. Schock et al. (1989) report that the [001] direction of olivine is about 0.3 log units higher in conductivity than the [010] direction at 1200° C and $f_{O_2} = 10^{-3}$ Pa.

The curves through the data points were fit using the model

$$\sigma = \sigma_0 + \sigma_1 f_{O_2}^c \qquad (8)$$

where σ is the conductivity, σ_0 is the conductivity independent of f_{O_2}, σ_1 is the preexponential term, and c is the exponent of the f_{O_2} dependence. This equation was used by Constable and Duba (1990) to describe the conductivity-f_{O_2} curves of their single and polycrystalline experimental results. Constable and Duba allowed σ_0, σ_1, and c to be free variables when fitting their data. The result is a very good fit to the data, but the exponent c was found to be 0.296 (the weighted average for their three data sets; Red Sea olivine, San Carlos olivine, and Jackson County dunite). This is much higher than the expected f_{O_2}-dependence of olivine conductivity based on point defect calculations (Stocker and Smyth 1978; Hirsch and Shankland 1991b) and other experimental determinations (Schock et al. 1989). Based on the above studies, the conductivity is expected to have a depen-

dence on f_{O_2} to the 1/5.5–1/7 (0.18–0.14) power. Because of its importance in interpreting electrical conduction in olivine, a brief discussion of defect chemistry and the recent defect model for olivine by Hirsch and Skankland (1991 b) is presented here.

Electrical conduction in olivine is largely dependent on temperature, composition, f_{O_2}, and defect chemistry. The defect equilibria in Fe-bearing olivine has been qualitatively described (e.g., Stocker 1978a, b, c; Stocker and Smyth 1978; Nakamura and Schmalzried 1983). The model presented by Hirsch and Shankland (1991a, b) is a computational model based on solving the set of coupled nonlinear equations that govern the defect populations using available thermodynamic data as model input. The result is a set of quantitative models of the concentration of each defect as a function of f_{O_2} for different temperatures and Fe content.

From Fig. 13 we note that at 1200° C the most concentrated defects in the range of f_{O_2} of our experiments are electrons, trivalent Fe on Mg sites ($Fe_{Mg}^{\bullet}$; the small polaron), oxygen interstitials (O_I''), Mg vacancies (V_{Mg}''), Mg interstitials ($Mg_I^{\bullet\bullet}$), and Si vacancies (V_{Si}''''). Here we employ standard Kröger-Vink notation (1956). The conductivity depends not only on the concentration of charged defect species, but also their mobilities. That is,

$$\sigma = \Sigma c_i q_i \mu_i \qquad (9)$$

where c_i is the concentration of the charge carrier, q_i is the charge, and μ_i is the mobility. In general, the conductivity is dominated by one defect species (Tuller 1985; Schock et al. 1989), in which case we expect a plot of the conductivity versus f_{O_2} to have an f_{O_2} dependence similar to that of the concentration of one of the defect species listed above. The conductivity of the grain interiors at 1200° C for the NCD and SQD both display a positive f_{O_2} dependence (Fig. 10), with a slope that approaches 1/5.5 at the highest f_{O_2}'s. The grain interiors of the NCD show similar f_{O_2} dependences at 1004 and 1101° C. Experimental measurement of the Seebeck coef-

ficient by Schock et al. (1989) indicates that the sign of the dominant charge carrier in single crystal San Carlos olivine is positive below 1390° C. According to the defect population model, the only positively charged defect existing in sufficient quantity to account for the observed conductivity is $Fe_{Mg}^{\bullet}$. The concentration of $Fe_{Mg}^{\bullet}$ depends on f_{O_2} to the 1/5.5 power which can be explained by considering the following defect reaction (Schock et al. 1989):

$$2O_2 + 8Fe_{Mg}^x = 4O_O^x + 2V_{Mg}'' + V_{Si}'''' + 8Fe_{Mg}^{\bullet}. \qquad (10)$$
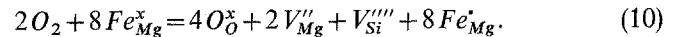
The equilibrium constant K_{10} for this reaction can be written as

$$K_{10}f_{O_2}^2 = (Fe_{Mg}^{\bullet})^8 (V_{Mg}'')^2 (V_{Si}'''') \qquad (11)$$

where the brackets refer to the concentration of the species. Assuming the charge balance condition $(Fe_{Mg}^{\bullet}) = 4(V_{Mg}'') = 8(V_{Si}'''')$ yields

$$(Fe_{Mg}^{\bullet}) = K_{10}' f_{O_2}^{1/5.5}. \qquad (12)$$

Of the most abundant defects considered by Hirsch and Shankland, $Fe_{Mg}^{\bullet}$ is the most abundant mobile charged species and displays the correct f_{O_2} dependence and sign of charge carrier to explain the observed experimental data. A complicating factor is the possible contribution to conduction of other defects. The mobility of e' may be as much as 1000 times higher than that of $Fe_{Mg}^{\bullet}$ whereas the mobility of V_{Mg}'' may be as low as 0.1 times the mobility of $Fe_{Mg}^{\bullet}$ (Hirsch and Shankland 1991b). The total effective charge carriers contributing to conduction would then be $1000\{e'\} + \{Fe_{Mg}^{\bullet}\} + 0.1\{V_{Mg}''\}$, which is plotted on Fig. 13. The effect is to modify the effective charge carrier curve at low f_{O_2}'s so that there is a 'flat' region independent of f_{O_2}, while $Fe_{Mg}^{\bullet}$ dominates conduction at higher f_{O_2}'s.

Because of experimental limitations, it is difficult to obtain results at f_{O_2}'s higher than 10^{-3} Pa at 1200° C, which means that measurements are made at f_{O_2}'s just to the point at which one would expect to see the 1/5.5
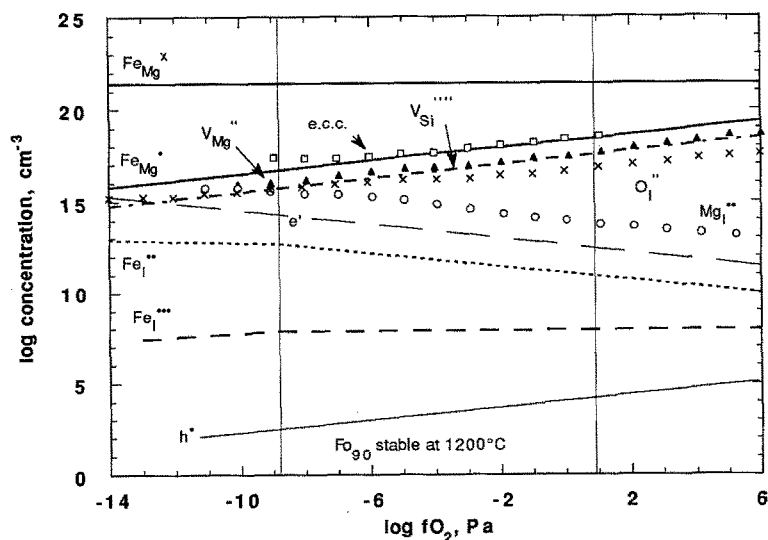

Fig. 13. The defect population model of Hirsch and Shankland (1991b) for Fo_{90} at 1200° C assuming a constant cation ratio (unbuffered by pyroxene) for several defect species. The Fo_{90} stable lines are from Nitsan (1974). Symbols: solid triangles, V_{Mg}''; open circles, $Mg_I^{\bullet\bullet}$; x's, O_I''; heavy solid line $Fe_{Mg}^{\bullet}$; light solid line, $h^{\bullet}$; long-dashed line, e'; dashed line, $Fe_I^{\bullet\bullet}$; dotted line, $Fe_I^{\bullet\bullet\bullet}$. The open squares, labeled e.c.c., represent the total of the effective charge carriers as calculated by Hirsch and Shankland and explained in the text. The grain interior conductivity of olivine displays and f_{O_2} dependence similar to the f_{O_2} dependence of the concentration of $Fe_{Mg}^{\bullet}$, and the effective charge carriers

Table 2. Fitting parameters to conductivity-f_{O_2} data using (8)

Material	Temp (°C)	$\log \sigma_0$ (S/m)	$\log \sigma_1$ (S/m)	%RMS
Grain interior mechanism, fixed exponent $c = 1/5.5$				
NCD1	1004	-4.20 ± 0.63	-3.10 ± 0.10	0.61
NCD2	1101	-4.02 ± 0.13	-2.99 ± 0.15	0.69
NCD3	1200	-3.70 ± 0.05	-2.77 ± 0.05	0.32
SQD5	1200	-3.40 ± 0.07	-2.90 ± 0.15	0.62
Grain interior mechanism, fixed exponent, $c = 1/7$				
NCD1	1004	-4.25 ± 0.11	-3.29 ± 0.13	0.74
NCD2	1101	-4.12 ± 0.24	-3.13 ± 0.18	0.82
NCD3	1200	-3.81 ± 0.09	-2.87 ± 0.07	0.43
SQD5	1200	-3.44 ± 0.08	-2.99 ± 0.14	0.58

Table 3. Fitting parameters to conductivity-f_{O_2} data using (13)

Material	Temperature (°C)	$\log \sigma_0$ (S/m)	Slope	%RMS
Grain boundary mechanism				
NCD1	1004	-3.90 ± 0.10	0.019 ± 0.014	0.90
NCD2	1101	-3.33 ± 0.09	-0.033 ± 0.015	1.07
NCD3	1200	-3.13 ± 0.34	-0.081 ± 0.060	7.49
SQD5	1200	-3.44 ± 0.05	0.008 ± 0.009	0.83
Grain interior mechanism, single crystal sample				
SC19	1001	-2.56 ± 0.48	0.134 ± 0.073	2.44

or $1/7 f_{O_2}$ dependence. What we observe is the flat region where the concentration of effective charge carriers remains constant, until with increasing f_{O_2}, the concentration depends on f_{O_2} to the 1/5.5 power. Experimentally, we do observe a gradual increase in the slope with increasing f_{O_2}, but not the full 1/5.5 dependence. For this reason we fit the high frequency grain interior data using (8) with the exponent c fixed at a value of 1/5.5 (theoretical) and 1/7 (experimental, (Schock et al. 1989)). The results of these analyses are presented in Table 2. The sin-

gle crystal data have been fit with a straight line equation ((13), next section) because of the lack of data points to get a meaningful fit using (8). The observed slope is 0.134 (Table 3), consistent with similar measurements made by Schock et al. (1989).

Grain Boundary Conductivity. The grain boundary conductivity of each experiment is plotted in Fig. 14. The equation

$$\sigma = \sigma_1 f_{O_2}^c \qquad (13)$$

was used to fit the data, and is a straight line on a log σ versus log f_{O_2} plot. σ_1 is the preexponential term and the exponent c is the slope. A straight line fit was used since there is no a priori reason to assume a different type of f_{O_2} dependence, and the data do not indicate any curvature. The values obtained from the fits are presented in Table 3. From Fig. 14 and Table 3 we note that $\sigma_{gb,SQD5}$ displays a very slight positive slope of 0.008, in contrast to $\sigma_{gb,NCD3}$ which has a slope of -0.081. Another interesting observation is that the slope of $\sigma_{gb,NCD}$ becomes increasingly negative as temperature increases. The mechanism responsible for grain boundary conduction is not known. There are very little data available on intergranular diffusion in polycrystalline olivine. Oxygen has been shown to diffuse relatively fast in polycrystalline dunite ($D \approx 10^{-7}$ cm^{-2}/s at 1200° C, 1 GPa) (Watson 1986). Because we expect that the concentration of oxygen on grain boundaries increases with increasing f_{O_2}, the negative or non-f_{O_2} dependence of the conductivity appears to rule oxygen defects out as the grain boundary mechanism. The only other study of intergranular diffusion in olivine of which we are aware is by Naughton and Fujkawa (1959). They determined that in polycrystalline olivine $D_{Fe,gb} \approx 10^{-11}$ cm^2/s at 1200° C, approximately the same rate as within the crystal lattice (Jurewicz and Watson 1988). The diffusion rate of Fe on grain boundaries is at least one order of magnitude too slow to account for the observed grain boundary conductivity in these studies.
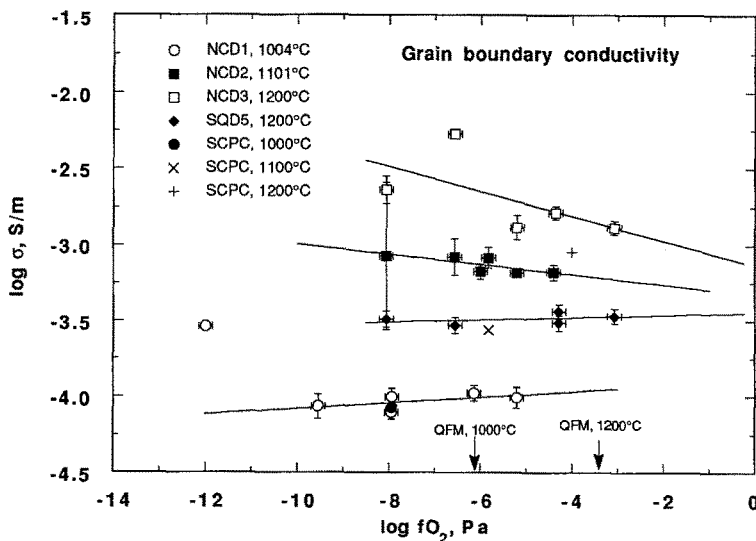

Fig. 14. Log σ_{gb} versus log f_{O_2} for all the polycrystalline experiments, including San Carlos polycrystalline compacts (SCPC; Roberts and Tyburczy 1991). The lines through the data are straight line fits using (13). The lowest f_{O_2} point for NCD1 is not included in the fit because of the uncertainty in this point. The fit parameters are listed in Table 3. As temperature increases, σ_{gb} of the NCD displays an increasingly negative slope. The grain boundaries of SQD5 show a slight positive f_{O_2} dependence at 1200° C. The arrows indicate f_{O_2}'s corresponding to the QFM buffer assemblage at 1000 and 1200° C
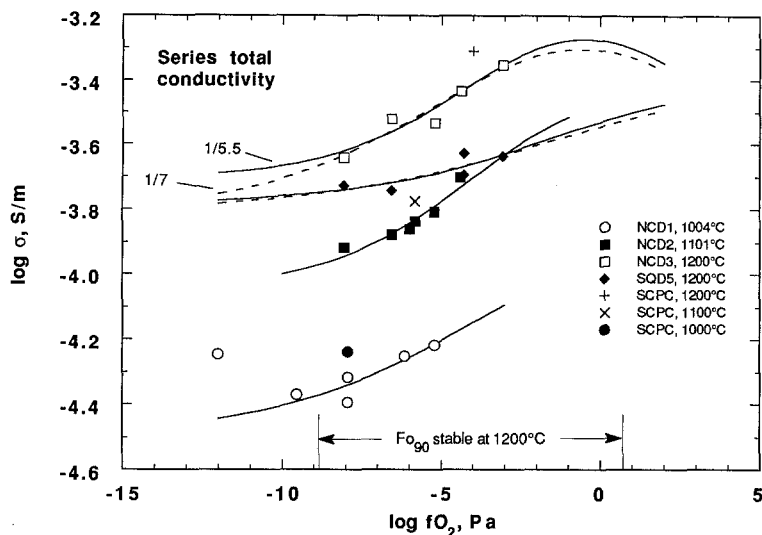
Fig. 15. Log σ_{total} versus log f_{O_2} for all the polycrystalline experiments, including San Carlos polycrystalline compacts (SCPC; Roberts and Tyburczy 1991). The total conductivity is the series sum of the grain interior and grain boundary conductivities. The *solid lines* through the data are the series sums of the fits to the grain interiors and grain boundaries separately, assuming an exponential f_{O_2} dependence of the grain interiors of $1/5.5$, *dashed lines* assume an exponential f_{O_2} dependence of $1/7$ for the grain interiors. Log σ_{total} for NCD3 (*open squares*) and SQD5 (*filled squares*) at 1200° C as a function of f_{O_2} are extrapolated to an extended range of f_{O_2}. The approximate stability field of Fo$_{90}$ at 1200° C is indicated at the bottom of the diagram (Nitsan 1974)

Total Conductivity of Polycrystalline Dunite. In both the SQ and NC dunites, the two conduction mechanisms add in series, resulting in a lower total conductivity than for either mechanism considered separately (Figs. 10, 11). The result is an f_{O_2} dependence for the total conductivity that is lower than the grain interior f_{O_2} dependence over the range of experimental measurement. The total DC conductivity as a function of f_{O_2} is shown in Fig. 15. The lines through the data on this graph are the series combination of the fits to σ_{gi} and σ_{gb} of (8, 13) assuming in $f_{O_2}^{1/5.5}$ dependence for the grain interiors such that

$$\sigma_{total} = (1/\sigma_{gi} + 1/\sigma_{gb})^{-1}. \tag{14}$$

For the 1200° C data, σ_{total} assuming the grain interior conductivity varies as f_{O_2} to the $1/7$ power is also plotted. Over the range of f_{O_2} of the experiments, this assumption has a minimal effect on the description of σ_{total}. However, when extrapolating to higher f_{O_2}'s this assumption can have a slightly greater effect on σ_{total}. The approximate stability field of Fo$_{90}$ at 1200° C calculated from Nitsan (1974) is illustrated on Fig. 15. On this diagram σ_{total} is plotted by extrapolating the f_{O_2} dependences of both grain interior and grain boundary conductivity as determined from the fits to the data in Tables 2 and 3 (Figs. 12, 14). At the higher f_{O_2} end of the stability region the total conductivity of NCD3 (1200° C) actually decreases with increasing f_{O_2}. This decrease is a result of the series behavior of the two conduction mechanisms and the negative, or lower f_{O_2} dependence of the grain boundary mechanism. The overall conductivity is controlled by the most resistive mechanism. When the two mechanisms are sub-equal, they both contribute to the total conductivity. If one mechanism is much more resistive than the other, the total conductivity is dominated by that mechanism. The slope of $\sigma_{gb,NCD}$ versus f_{O_2} becomes increasingly negative with increasing temperature. If this trend continues at higher temperatures, the effect demonstrated above where σ_{total} displays a negative slope at the higher f_{O_2}'s will be increased. We caution that further experiments are needed to determine the f_{O_2} de-

pendence of both grain interior and grain boundary mechansims at the highest f_{O_2}'s of the Fo$_{90}$ stability field and suggest that care be used when extrapolating the results of this study to higher f_{O_2} regions.

Discussion

The f_{O_2} dependence of the grain interior conductivity is similar to that seen in other experimental studies and predicted by chemical defect calculations. Defect modeling predicts that the concentration of $Fe^\bullet_{Mg}$ (and effective charge carriers) will shift to higher f_{O_2}'s with increasing temperature (Hirsch and Shankland 1991b). The experimental results of this study (Fig. 12) agree with this prediction. The SQD, higher in Fe content than NCD, does not display as strong an f_{O_2} dependence as NCD at the highest f_{O_2}'s over the same range of f_{O_2}. The grain boundaries display a negative f_{O_2} dependence. Grain boundary regions are an area of intense research and high interest in materials science. The structural, diffusive and electrical properties of a large number of polycrystalline compounds have been studied, but little research has been performed on silicates. A number of parallels can be made by comparing results from materials science to the results of this study.

The idea that grain boundaries in polycrystalline materials representative of the upper mantle will enhance the electrical conductivity of those materials is not supported by the results of this study. In the dunites studied here we find that the grain boundary resistivity adds in series with the grain interior resistivity, resulting in a higher DC resistivity (lower conductivity) for the material. Materials such as Al_2O_3, MgO, ZrO_2, and numerous other oxides demonstrate a similar grain boundary response. This type of series behavior is caused by the higher dielectric permittivity, and hence the higher capacitance, of the grain boundaries as compared to the grain interiors. The phenomenon of grain boundaries occurring in series with grain interiors resulting in a more resistive material is termed the "grain boundary effect"

(Gerhardt and Nowick 1986). Gerhardt and Nowick studied the grain boundary effect in doped ceria (dopants Y, Gd, and La), an ionic conductor, and determined that $\sigma_{total,DC}$ could be reduced by up to three orders of magnitude by this effect. The formation of a silica phase at the grain boundaries was found to be the cause of the resistive grain boundary arc. An interesting aspect of their study (that may be applicable to silicate Earth materials) is that the grain boundary effect could be nearly eliminated by using ultra-pure materials free of silica and minimized by utilizing high dopant concentrations and doping cations of large ionic radius. Grain boundaries are thought to be blocking to electronic conduction mechanisms (Schock et al. 1977). Fo_{90} is thought to be an electronic conductor below 1390° C and an ionic conductor at temperatures above 1390° C (Schock et al. 1989). This could indicate that charge blocking at grain boundaries might be eliminated at temperatures greater than 1400° C. Earlier work on the complex impedance of San Carlos olivine compacts demonstrated that σ_{gb}/σ_{gi} increased with increasing temperature, and that above 1344° C $\sigma_{gb} > \sigma_{gi}$, consistent with the above scenario (Roberts and Tyburczy 1991).

That the grain boundary region is an area containing a large degree of disorder is generally agreed upon. Grain boundaries can also display a definite periodicity and composition. Furthermore, impurity segregation is commonly observed at grain boundaries. Duffy (1986) reports that in ionic crystals (such as NiO) the mechanism responsible for diffusion in grain boundaries and in the bulk appears to be the same. In olivine, grain boundary diffusion of Fe and lattice diffusion of Fe are on the same order of magnitude (Naughton and Fujikawa 1959; Jurewicz and Watson 1988; Nichols and Mackwell 1991). Grain boundary and grain interior conduction mechanisms in the polycrystalline dunites studied here may not be identical as evidenced by the distinctly different f_{O_2} dependence of the crystal interior versus the grain boundary conductivities. Two possibilities are 1) there are two different conduction mechanisms (i.e., different "defects" or ions) responsible for grain interior and grain boundary conduction, or 2) the diffusivity and/or mobility of the "defects" or ions is different within the crystal lattice and on the grain boundary. It may be possible to learn more about the nature of the grain boundary mechanism by performing additional conductivity, diffusion, and thermopower experiments, and by analytically determining the composition of the grain boundaries. One possible reason for reduced defect mobility within grain boundaries is the presence of a high number of dangling bonds at grain boundaries (Grovenor 1985) that can serve as charge and defect traps that inhibit diffusion.

Another way of considering grain boundaries is as an amorphous region (Chiou et al. 1989). An amorphous region such as a glass or melt would be similar to a grain boundary in that they are both highly disordered regions and they both are areas where diffusion, at least in some materials, may occur quickly. The grain boundaries in this study have a much lower conductivity than a glass or melt. We cannot directly compare $\sigma_{gb,bulk}$ of

this study to σ_{glass}, because $\sigma_{gb,bulk}$ is a volume weighted value of $\sigma_{gb,micro}$. This is illustrated by the observed series electrical behavior of the grain interior and grain boundary mechanisms. The bricklayer model (van Dijk and Burggraaf 1981; Verkerk et al. 1982b; Bonanos et al. 1987) has previously been used to describe conduction in polycrystalline olivine (Roberts and Tyburczy 1991). This model treats the material under study as a two phase mixture of cubic grains surrounded everywhere by the grain boundary 'phase'. There are two end member paths of conduction within this model: 1) through a grain, across a grain boundary and through a grain repeatedly, and 2) through a grain boundary only, bypassing the grains. In light of this model, DC resistivities in series add according to

$$\rho_{total} = (x_{gi}) \rho_{gi} + (x_{gb}/3) \rho_{gb,mic} \tag{15}$$

where x_{gb} is the volume fraction of the grain boundary phase, x_{gi} is the volume fraction of the grain interiors $(x_{gi} \approx 1)$, $\rho_{gb,mic}$ is the microscopic grain boundary resistivity (that is, the resistivity of pure grain boundary 'phase'), and the factor of three arises because on the average, only 1/3 of the grain boundary phase is in the series path. x_{gb} is estimated by

$$x_{gb} = \frac{3D^2 d + 3D d^2 + d^3}{D^3 + 3D^2 d + 3D d^2 + d^3}, \tag{16}$$

where D is the length of a side of a cubic grain and d is the grain boundary width. For our experiments on SQD $D \approx 300$ µm, and we estimate $d \approx 10$ nm. For $D \gg d$, $x_{gb} \approx 3d/D$. From Tyburczy and Waff (1983) we can estimate a resistivity of basaltic melt (Hawaiian tholeiite) at 1200° C of 0.5 Ωm. With these parameters, equation 15 yields a value of $\rho_{total} = \rho_{gi} + 1.7 \times 10^{-5}$ Ωm. Since ρ_{gi} is on the order of 10^3 Ωm, $\rho_{total} = \rho_{gi}$. Assuming a wider grain boundary width of 1 µm, $\rho_{total} = \rho_{gi} + 1.7 \times 10^{-3}$ Ωm, which is essentially the same result, meaning that if the conductivity of grain boundaries is similar to that of a melt, they would contribute nothing to the total resistivity of a sample that exhibits series electrical behavior. Alternatively, if the grain boundaries behave similar to a melt and exhibit parallel conduction behavior with the grain interiors, the conductivities add according to

$$\sigma_{total} = (x_{gi}) \sigma_{gi} + (2 x_{gb}/3) \sigma_{gb,mic}. \tag{17}$$

Here the factor of 2/3 arises because two-thirds of the grain boundary 'phase' is in parallel with the grain interiors and we have assumed cubic grains. Using the same parameters as before ($\sigma_{gi} \approx 10^{-3}$ S/m, $\sigma_{gb,mic} = 2$ S/m, $D = 300$ µm, $d = 10$ nm), $\sigma_{total} = \sigma_{gi} + 1.3 \times 10^{-4}$ S/m; $\approx 1.13 \times 10^{-3}$ S/m. For a wider grain boundary of 1 µm, $\sigma_{total} = \sigma_{gi} + 1.3 \times 10^{-2}$ S/m; $\approx 1.4 \times 10^{-2}$ S/m. If parallel behavior occurs, only one impedance arc will be observed in the complex impedance plane (excluding the electrode response). Experimentally this is not observed, ρ_{gb} adds in series with ρ_{gi} and the grain boundaries have a much higher resistivity than silicate melts at similar conditions. Thus we conclude that the grain boundary

microscopic conductivity is much less than that of a basaltic glass. For a minority phase such as a grain boundary to enhance bulk conduction, that phase must have a significantly higher conductivity than the grain interiors ($\sigma_{gb,mic} \geq 10^3 \sigma_{gi}$), and must conduct in parallel with the grain interiors ($\tau_{gb} \approx \tau_{gi}$).

In terms of polycrystalline materials as analogs of mantle rocks, xenoliths such as those found at San Quintin and San Carlos probably better represent a sample of the upper mantle than alpine peridotite bodies like the Jackson County peridotite. Earlier work performed on polycrystalline compacts of San Carlos olivine also indicates series electrical behavior for grain interior and grain boundary mechanisms (Tyburczy and Roberts 1990; Roberts and Tyburczy 1991). The grain interiors of the polycrystalline compacts are more conductive than those of the natural dunites of the present work (Fig. 12). The grain boundaries of the polycrystalline compacts are more resistive than $\sigma_{gb,NCD}$, slightly more conductive than $\sigma_{gb,SQD}$ at 1200° C, and nearly equal to $\sigma_{gb,NCD}$ at 1100 and 1000° C (Fig. 14). The resulting total conductivity of the polycrystalline olivine compacts is greater than either natural dunite (Fig. 15). Tyburczy and Roberts also showed that from 800 to approximately 1250° C $\sigma_{gb} < \sigma_{gi}$, and from 1250 to 1400° C $\sigma_{gb} > \sigma_{gi}$. The ratio of grain interior to grain boundary conductivities of the San Quintin dunite displays the opposite temperature dependence. At 900° C the SQD has more conductive grain boundaries than grain interiors, and at 1200° C the grain interiors are more conductive than the grain boundaries. The material with the most conductive grain boundaries is the North Carolina dunite. The ratio of σ_{gb}/σ_{gi} increases with increasing temperature for this material. In the natural rocks studied, the grain boundary electrical response always acts in series with the grain interior response. However, the value of σ_{gb}, the relationship of σ_{gb} to σ_{gi}, and the f_{O_2} dependence of σ_{gb} exhibit considerable variability.

Conclusions

The role of grain boundaries in determining the electrical properties of a material is dependent upon many factors, including temperature, composition, and f_{O_2}. Only by making complex impedance measurements at frequencies as low as 10^{-3} to 10^{-4} Hz are we able to distinguish grain boundary contributions and determine their separate response to different experimental conditions. By modeling the electrical response with equivalent circuits of resistors and capacitors we are able to determine the separate conductivities of both grain interiors and grain boundaries. The conductivity of the grain interiors displays a positive f_{O_2} dependence, approaching an exponential dependence of 1/5.5 at the most oxidizing f_{O_2}'s within the olivine stability field. This behavior is in agreement with previous experimental and theoretical determinations. The electrical response of the grain boundaries is observed at lower frequencies than that of the grain interiors, between approximately 10^{-3} to 10^3 Hz. It is necessary to make measurements at frequen-

cies lower than this to accurately assess the sample-electrode effects on the complex impedance. Series electrical behavior is exhibited by the grain boundaries and grain interiors indicating very different relaxation times. The grain boundaries exhibit a different f_{O_2} dependence than the grain interiors. The grain boundary conductivity of the North Carolina dunite is greater than the grain interior conductivity and displays an increasingly negative f_{O_2} dependence with increasing temperature. The grain boundaries of the San Quintin dunite are more resistive than the grain interiors and display a slightly positive f_{O_2} dependence. The grain boundaries of ground-and-pressed compacts of San Carlos olivine also exhibit resistive grain boundaries in series with grain interiors (Tyburczy and Roberts 1991). Because of the variable and sometimes negative f_{O_2} dependence of the grain boundary conductivity, we conclude that the mechanism of charge transport is probably not oxygen ion transport. The grain boundary charge transport mechanism remains to be determined. Mantle materials probably have grain boundaries most like the San Quintin dunite, and from this we might expect that the grain boundaries of mantle materials will behave in a similar manner electrically, exhibiting grain boundaries that are more resistive than the grain interiors that add in series with grain interiors. The effect of resistive, charge blocking grain boundaries on the total conductivity of a polycrystalline olivine may be reduced at temperatures above 1400° C.

References

Astwood PM, Carpenter JR, Sharp WE (1972) A petrofabric study of the Dark Ridge and Balsam Gap dunites, Jackson County, North Carolina. Southeastern Geol 14:183–194

Basu AR (1977) Olivine-spinel equilibria in lherzolite xenoliths from San Quintin, Baja California. Earth Planet Sci Lett 33:443–450

Basu AR, Murthy VR (1977) Ancient lithospheric lherzolitic xenolith in alkali basalt from Baja California. Earth Planet Sci Lett 35:239–246

Bauerle JE (1969) Study of solid electrolyte polarization by a complex admittance method. J Phys Chem Solids 30:2657–2670

Bonanos N, Steele BCH, Butler EP (1987) Characterization of materials. In: Macdonald JR (ed) Impedance Spectroscopy. Wiley, New York, pp 191–237

Chiou BS, Lin ST, Duh JG, Chang PH (1989) Equivalent circuit model in grain-boundary barrier layer capacitors. J Am Ceram Soc 72:1967–1975

Chu SH, Seitz MA (1978) The ac electrical behavior of polycrystalline ZrO2-CaO. J Sol St Chem 23:297–314

Constable SC, Duba AG (1990) The electrical conductivity of olivine, a dunite and the mantle. J Geophys Res 95:6967–6978

Duffy DM (1986) Grain boundaries in ionic crystals. J Phys C 19:4393–4412

Grovenor CRM (1985) Grain boundaries in semiconductors. J Phys C 18:4079–4119

Gudmundsson G, Holloway JR (1992) Activity-composition relationship in the system Fe-Pt at 1300 and 1400° C and at 1 atm and 20 kbar. Am Mineral (in press)

Haak V (1982) A comparison of the electrical conductivity of natural mono- and polycrystalline olivines – A case to decide. In Schreyer W (ed) High-Pressure Researches in Geoscience. E Schweizerbart'sche Verlagsbuchhandlung, Stuttgart pp 407–417

Hirsch LM, Shankland TJ (1991a) Determination of defect equilibria in minerals. J Geophys Res 96:377–384

Hirsch LM, Shankland TJ (1991b) Quantitative olivine defect chemical model: Insights on electrical conduction, diffusion, and the role of Fe impurities. Geophys J Int (in press)

Hurt RL, Macdonald JR (1986) Distributed circuit elements in impedance spectroscopy: A unified treatment of conductive and dielectric systems. Solid State Ion 20:111–124

Jurewicz AJG, Watson EB (1988) Cations in olivine, Part 2: Diffusion in olivine xenocrysts, with applications to petrology and mineral physics. Contrib Mineral Petrol 99:186–201

Kariya KA, Shankland TJ (1983) Electrical conductivity of dry crustal rocks. Geophysics 48:52–61

Kröger FA, Vink HV (1956) Relations between the concentrations of imperfections in crystalline solids. Solid State Phys 3:307–435

Lilley E, Strutt JE (1979) Bulk and grain boundary ionic conductivity in polycrystalline β''-alumina. Phys Status Solidi 54:639–650

Macdonald JR, Schoonman J, Lehnen AP (1982) The applicability and power of complex nonlinear least squares for the analyses of impedance and admittance data. J Electroanal Chem 131:77–95

Macdonald JR (1985) Generalizations of "universal dielectric response" and a general distribution-of-activation-energies model for dielectric and conducting systems. J Appl Phys 58:1971–1978

Nakamura A, Schmalzried H (1983) On the nonstoichiometry and point defects of olivine. Phys Chem Minerals 10:27–37

Naughton JJ, Fujikawa U (1959) Measurement of intergranular diffusion in a silicate system: Iron in forsterite. Nature 184:54–56

Nichols SL, Mackwell SJ (1991) Grain growth in porous olivine aggregates. Phys Chem Minerals 18:269–278

Nitsan U (1974) Stability field of olivine with respect to oxidation and reduction. J Geophys Res 79:706–711

Olhoeft GR (1979) Electrical properties. In Hunt GR, Johnson GR, Olhoeft GR, Watson DE, Watson K (eds) Initial Report of the Petrophysics Laboratory. Geological Survey Circular 789, US Geological Survey, Washington, DC, pp 1–26

Olhoeft GR (1985) Low frequency electrical properties. Geophysics 50:2492–2503

Raistrick ID (1987) The elctrical analogs of physical and chemical processes. In: Macdonald JR (ed) Impedance Spectroscopy. Wiley, New York, pp 27–84

Roberts JJ, Tyburczy JA (1991) Frequency dependent electrical properties of polycrystalline olivine compacts. J Geophys Res 96:16,205–16,222

Roberts JJ, Tyburczy JA (1992) Impedance spectroscopy of single and polycrystalline olivine: Evidence for grain boundary transport. Phys Chem Minerals (in press)

Schock RN, Duba AG, Heard HC, Stromberg HD (1977) The electrical conductivity of polycrystalline olivine and pyroxene under pressure. In: Manghnani M, Akimoto S (eds) High-Pressure Research: Applications in Geophysics. Academic, San Diego, pp 39–51

Schock RN, Dubna AG, Shankland TJ (1989) Electrical conduction in olivine. J Geophys Res 94:5829–5839

Shankland TJ, Waff HS (1977) Partial melting and electrical conductivity anomalies in the upper mantle. J Geophys Res 82:5409–5417

Skankland TJ (1981) Electrical conduction in mantle materials. In O'Connell RJ, Fyfe WS (eds) Evolution of the Earth. Geodyn Ser, vol 5, AGU, Washington DC, pp 256–263

Stocker RL (1978a) Influence of oxygen pressure on defect concentrations in olivine with a fixed cationic ratio. Phys Earth Planet Inter 17:118–129

Stocker RL (1978b) Point defect parameters in olivine. Phys Earth Planet Inter 17:108–117

Stocker RL (1978c) Variation of electrical conductivity in enstatite with oxygen partial pressure: Comparison of observed and predicted behavior. Phys Earth Planet Inter 17:P34–P40

Stocker RL, Smyth DM (1978) Effect of enstatite activity and oxygen partial pressure on the point-defect chemistry of olivine. Phys Earth Planet Inter 16:145–156

Tanaka J, Baumard J, Abelard P (1987) Nonlinear electrical properties of grain boundaries in an oxygen-ion conductor ($CeO_2 \cdot Y_2O_3$). J Am Ceram Soc 70:637–643

Tuller HL (1985) Electrical conduction in ceramics: Toward improved defect interpretation. In Schock RN (ed) Point Defects in Minerals. Geophysical Monograph 31, American Geophysical Union, Washington DC, pp 47–68

Tyburczy JA, Waff HS (1983) Electrical conductivity of molten basalt and andesite to 25 kilobars pressure: Geophysical significance and implications for charge transport. J Geophys Res 88:2413–2430

Tyburczy JA, Roberts JJ (1990) Low frequency electrical response of polycrystalline olivine compacts: Grain boundary transport. Geophys Res Lett 17:1985–1988

van Dijk T, Burggraaf AJ (1981) Grain boundary effects on ionic conductivity in ceramic GdxZr1-x02-(x/2) solid solutions. Phys Status Solidi 63:229–240

Verkerk MJ, Winnubst AJA, Burggraaf AJ (1982a) Effect of impurities on sintering and conductivity of yttria-stabilized zirconia. J Mat Sci 17:3113–3122

Verkerk MJ, Middelhuis BJ, Burggraaf AJ (1982b) Effect of grain boundaries on the conductivity of high-purity ZrO2-Y2O3 ceramics. Solid State Ion 6:159–170

Watson EB (1986) An experimental study of oxygen transport in dry rocks, and related kinetic phenomena. J Geophys Res 91:14117–14131